Journal of Materials Chemistry A

ROYAL SOCIETY OF CHEMISTRY

PAPER

View Article Online
View Journal

Cite this: DOI: 10.1039/d5ta10299e

Generating green hydrogen *via* nickel sulfide modified titania thin film photocatalysts

Melissa Sophie Egger, [a] Stephen Nagaraju Myakala, [b] Marco Sigl, [a] Georg Haberfehlner, [c] Manfred Nachtnebel, [d] Anto Vrbat, [e] Thomas Griesser, [e] Alaaddin Cem Ok, [bf] Alexey Cherevan, [b] Dominik Eder, [b] Thomas Rath *[a] and Gregor Trimmel *[a]

The emerging field of photocatalysis is a promising technology to pave the way to a greener future: photocatalytic water splitting can be used to synthesize green hydrogen. For this purpose, we modified mesoporous thin films of the well-known photocatalyst titania with a nickel sulfide cocatalyst prepared from nickel xanthate single source precursors *via* solution processing. Scanning transmission electron microscopy images of a sample cross-section revealed homogeneously deposited NiS nanoparticles throughout the whole titania layer. UV-Vis spectroscopy showed an increased light absorption of the NiS-modified titania samples into the visible range up to 600 nm. The photocatalytic performance of the modified catalyst films was evaluated using hydrogen evolution experiments with methanol as sacrificial electron donor. During those experiments, we observed a partly reversible color change of the catalysts, which we relate to an activation-deactivation mechanism. With an optimal NiS loading of 2.2 w%, we achieved the highest hydrogen evolution rate, averaging 3.3 mmol h^{-1} g^{-1} over twenty hours under near-UV light at 365 nm. This corresponds to an efficiency almost 250 times higher than that of the pristine titania and reaching 55% of the hydrogen evolution rate of titania modified with a similar amount of platinum cocatalyst. The obtained rate, combined with the vast difference in cost of platinum and nickel, is a promising result to enable the production of green solar fuels.

Received 17th December 2025
Accepted 23rd March 2026

DOI: 10.1039/d5ta10299e

rsc.li/materials-a

Introduction

Hydrogen is an increasingly important industrial resource: from 2000 to 2020, the global hydrogen demand increased from approximately 60 to 90 Mt.[1] Almost all of the hydrogen finds use in the traditional applications such as refining, as reducing agent in the steel industry, or as feedstock in the chemical industry. In the chemical industry, the majority applications are the production of ammonia (used to produce nitrogen fertilizer) or methanol. Only a very small part falls currently within new application sectors such as transportation, hydrogen-based fuels, or electricity generation and storage. Moreover, hydrogen is currently produced mainly from fossil sources (natural gas (59%), coal (19%)), or as by-product of other industrial processes.[1] All of those routes produce high amounts of carbon dioxide in the process. In addition, the hydrogen obtained from steam reforming of natural gas contains impurities such as carbon monoxide. For applications such as fuel cells, which require high purity hydrogen, further purification is needed.[2]

Green hydrogen can be produced by water splitting.[3] Water electrolysis does not emit carbon dioxide, however, with an energy efficiency of approximately 60–90% there is a significant loss of energy involved.[4] When non-green electricity sources are used, this renders the net carbon dioxide emission even higher than for the direct conversion of natural gas to hydrogen.[3] Therefore, only the use of renewable energy to power electrolysis makes sense from a sustainability perspective. Still, even when using photovoltaics to power water electrolysis, a solar-to-hydrogen efficiency of 12.6% from a 17.3% efficiency silicon solar panel means a significant loss of energy in conversion.[3,5] A possibility to avoid this intermediate step of producing solar electricity is to directly convert sunlight into hydrogen by using photocatalysis, a rapidly developing field of research.[6–8]

Titania is the most researched photocatalyst, being cheap, non-toxic, and abundant. However, shortfalls such as low utilization of visible light, fast charge-carrier recombination,

[a]Institute for Chemistry and Technology of Materials (ICTM), NAWI Graz, Graz University of Technology, Stremayrgasse 9, 8010 Graz, Austria. E-mail: thomas.rath@tugraz.at; gregor.trimmel@tugraz.at
[b]Institute of Materials Chemistry, TU Wien, Getreidemarkt 9, 1060 Vienna, Austria
[c]Institute of Electron Microscopy and Nanoanalysis (FELMI), Graz University of Technology, Steyrergasse 17, 8010 Graz, Austria
[d]Graz Centre for Electron Microscopy (ZFE), Steyrergasse 17, 8010 Graz, Austria
[e]Institute of Chemistry of Polymeric Materials, Montanuniversität Leoben, Otto-Glöckel-Straße 2, 8700 Leoben, Austria
[f]Department of Metallurgical and Materials Engineering, Faculty of Engineering, Marmara University, TR-34722 Istanbul, Turkey

and a large hydrogen evolution overpotential limit its efficiency.[9–11] To address these issues, titania requires a cocatalyst. In such a binary catalyst/cocatalyst heterojunction system, the cocatalyst can take several roles: it can act as a sensitizer, promoting light harvesting over a larger range of the visible spectrum, or act as electron sink, which separates electron–hole pairs and suppresses charge recombination.[12] In addition, the cocatalyst can act as a provider of active catalytic sites that facilitate a desired reaction. Noble metals such as platinum or palladium are highly effective cocatalysts, especially for catalyzing hydrogen evolution.[9] Unfortunately, the use of noble metals renders a photocatalyst anything but cheap. The exploration of alternatives to lower cost and increase availability has brought forward metal sulfides as a feasible option.[10,13,14]

Nickel sulfide is a non-toxic and inexpensive metal sulfide with a narrow band gap of 0.3–0.5 eV for bulk NiS.[15] Due to its optoelectronic properties, it is typically not used as a standalone photocatalyst but rather as a cocatalyst to enhance the efficiency of other wide-bandgap semiconducting photocatalysts. For example, Shen *et al.* synthesized a composite of copper zinc sulfide with a mixed α-NiS-β-NiS phase.[16] The mixed NiS phases allowed to harness both the higher capacity of α-NiS for H_2O decomposition and the better conductive behavior of β-NiS. Furthermore, their study revealed that NiS acts mostly as electron acceptor rather than producing photoelectrons, thus reinforcing the role of NiS as a cocatalyst instead of as a standalone photocatalyst. Other reported NiS-based heterojunction photocatalyst systems include NiS/CdS,[17] NiS/TiO_2,[18,19] NiS/ZnS,[20] and NiS/ZrO_2.[21]

Nickel sulfide can be prepared by different methods, including the hydro- or solvothermal synthesis,[22] or the synthesis from single-source precursors such as nickel thiolate[23] or nickel xanthate.[24,25] The xanthate method is very attractive for the preparation of metal sulfides from solid state or dissolved precursors by thermal conversion. Further advantages of the xanthate method are its simplicity, combined with being reproducible and highly tunable.[24] Some examples highlighting the versatility of this method are CuS/SnS/ZnS (used for printing of semiconductors on paper),[26] CdS or $CuInS_2$ (used for the formation of polymer-inorganic solar cell active layers),[27,28] α-β-NiS (used for electrocatalytic water splitting),[29] γ-Ga_2S_3,[30] and ternary sulfides such as $AgSbS_2$ (ref. 31) or $ZnIn_2S_4$ (used for photocatalytic dye degradation).[32]

The use of thin film photocatalysts presents some advantages compared to catalysts used in suspension: the use in continuous photocatalysis is simplified, as the thin film system removes the need for both stirring and separation present in a suspension system.[33] At the moment, publications of thin film photocatalysts for hydrogen evolution are only sparsely available. The results, however, are very promising. Remarkable efficiencies were obtained for Pt@TiO_2 (90 mmol h^{-1} g^{-1}),[34] Pd@TiO_2 (104 mmol h^{-1} g^{-1}),[35] or ternary systems such as MoP/CdS@TiO_2 (35.5 mmol h^{-1} g^{-1})[33] and CdS@$TiO_{2,\ anatase}$@$TiO_{2,\ rutile}$ (57.95 mmol h^{-1} g^{-1}).[36]

Motivated by the promise of NiS cocatalysts and the possibility to capitalize on its facile fabrication *via* the xanthate route, we report the fabrication of mesoporous titania thin films featuring very thin coatings of nickel sulfide nanocrystals. The porous titania catalyst was infiltrated with a nickel xanthate precursor solution, which then was thermally converted to the nickel sulfide. We evaluated the photocatalytic performance of NiS@TiO_2 catalysts using hydrogen evolution experiments with methanol as sacrificial electron donor. The best result was obtained for a 2.2 w% NiS@TiO_2 film, which exhibited an average hydrogen evolution rate of 3.3 mmol h^{-1} g^{-1} over 20 hours under near-UV light at 365 nm.

Results and discussion

Preparation and characterization of the thin film catalysts

We synthesized nickel xanthates Ni(S_2C–O–R)$_2$ with different alkyl groups R for the NiS cocatalyst according to previously reported procedures.[37] As studied in a previous report, the organic moiety (linear: ethyl, *n*-propyl, *n*-pentyl; branched: isopropyl, isobutyl, and neopentyl) influences both the decomposition temperature of the xanthates and the preferred formed NiS crystal structure (α- and β-NiS, see SI Fig. S1),[24] which might be of interest to control the resulting photocatalytic performance. The structures and abbreviations of the xanthates, as well as a schematic workflow of the preparation of the thin film photocatalysts, are given in Fig. 1. Titania thin films on glass supports were prepared *via* blade coating of a commercial titania paste. After sintering at 500 °C, the titania films were modified with different nickel xanthate precursors in varying amounts by infiltration and subsequent thermal conversion. The isobutyl-xanthate NiXaC4b was selected as standard precursor and was used for most of the optimization experiments. Finally, a comparative series using all the listed xanthates were prepared with identical NiS-loading. The detailed description of the preparation can be found in the experimental section.

X-ray diffraction (XRD)

The XRD investigations of the thin film catalysts reveal only reflections from the anatase TiO_2 phase for both the pristine and the NiS-modified titania films (Fig. 2, blue and purple trace). The XRD measurement of the film prepared from only the xanthate precursors on glass shows sharp peaks corresponding to a mixture of α- and β-NiS (NiXaC4b precursor, Fig. 2, red trace). Thus, we assume that the absence of these reflections from the composite indicates that the amount of NiS in the TiO_2 matrix is too low for determination by XRD. However, we were able to detect the NiS nanocrystals using scanning transmission electron microscopy (see below, Fig. 3). Despite not being able to detect the state of NiS on our NiS@TiO_2 films, we expect that the sintering temperature and the xanthate precursor alkyl chain still influence the phase composition of the resulting NiS. At the sintering temperature of 400 °C used in this work, different mixtures of α-NiS and β-NiS or pure β-NiS are obtained depending on the used precursor.[24] The XRD measurements of pure NiS reference thin films obtained from all the precursors used in this work are given in the SI (Fig. S1). Shen *et al.* reported favorable results in photocatalytic hydrogen evolution efficiencies for the mixed-phase NiS cocatalyst compared to phase-pure β-NiS.[16] Therefore, we chose the isobutyl derivative NiXaC4b as standard

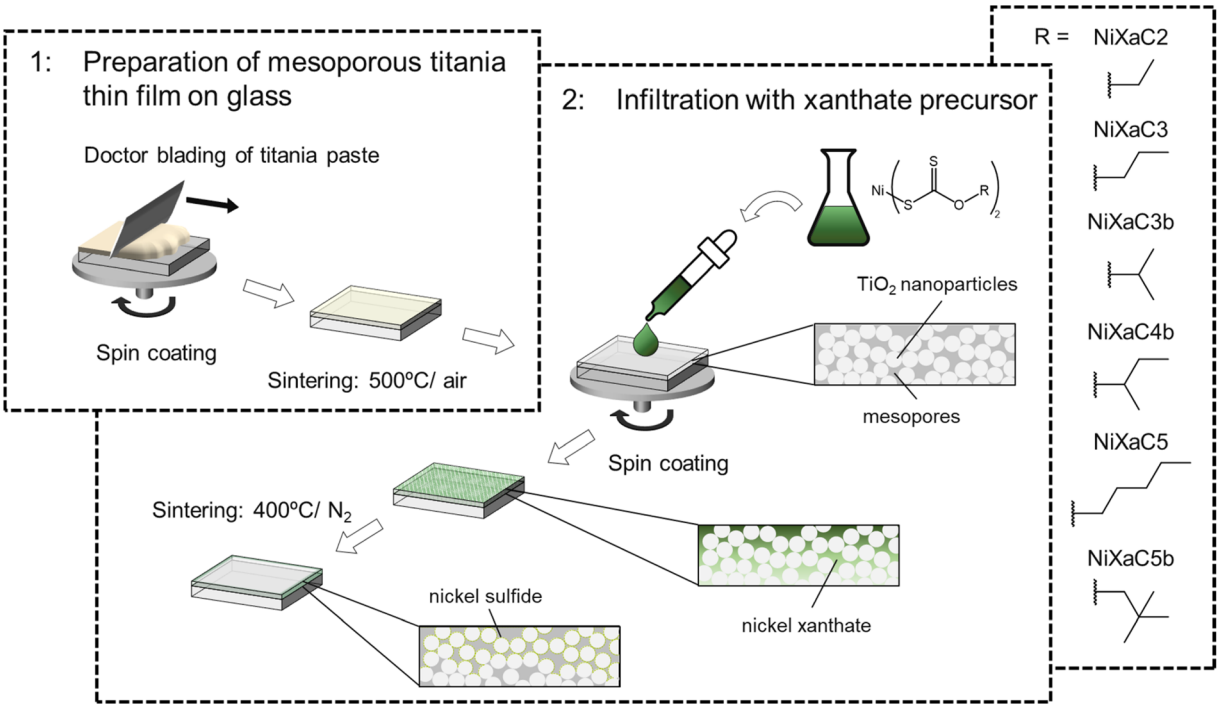

Fig. 1 Schematic depiction of the NiS@TiO_2 thin film catalyst preparation.

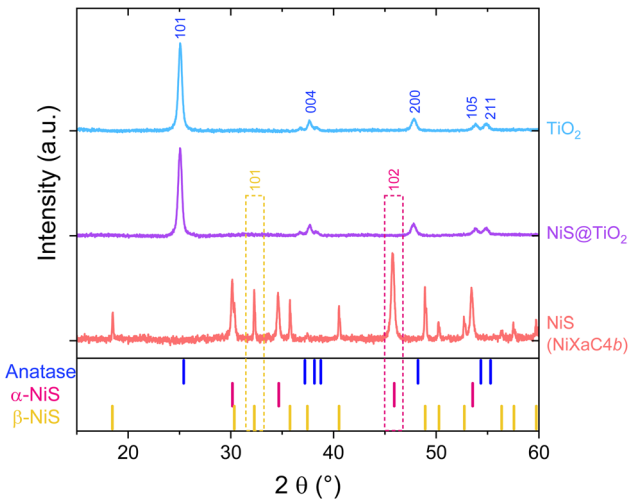

Fig. 2 X-ray diffractograms of the pristine mp-TiO_2 thin film, the NiS@TiO_2 thin film with the highest amount of NiS, and a drop coated NiS film prepared from the precursor NiXaC4b, with references for anatase TiO_2 (blue, PDF 00-021-1272), α-NiS (pink, PDF 01-075-0613), β-NiS (yellow, PDF 01-086-2280).

precursor for further characterizations, as it combines the resulting mixed phase NiS with sufficient solubility in chloroform, and a simple synthesis.

Scanning transmission electron microscopy (STEM)

To confirm the presence of NiS nanocrystals within the mesoporous TiO_2 scaffold, we recorded STEM images of a cross section of a NiS@TiO_2 film on glass. A high-angle annular dark-field (HAADF) image and energy dispersive X-ray spectroscopy (EDS) elemental mappings are depicted in Fig. 3. In the EDS mappings of nickel and sulfur, NiS is clearly visible as distinct nanocrystals with sizes of 7.6 ± 3.3 nanometers (SI, Fig. S2), which are homogeneously distributed within the mesoporous TiO_2 film. Due to the small size and the comparatively low amount of the NiS nanocrystals compared to TiO_2 (see below), it is plausible that the XRD patterns shows only the reflections of the TiO_2 scaffold. Furthermore, TEM images of the titania film with different magnifications are shown in Fig. S3 (SI). They reveal the homogeneous mesoporous structure expected from the employed titania nanoparticle paste (SI, Fig. S3B) and the interplanar spacings of the 101 and 105 lattice fringes of anatase (SI, Fig. S3C and D).

To further investigate the morphology and the elemental distribution within the 3.2 μm thick NiS@TiO_2 film, we studied larger parts of the cross section as shown in Fig. 4A and B. When looking at the very surface region of the cross section, the protection layer consisting of the heavier atoms platinum and gold appears in the HAADF-STEM as a very bright region (Fig. 4A). This bright area at the surface is also mirrored in the elemental distributions (SI, Fig. S4, area of the elemental mapping indicated by a rectangle in Fig. 4A), with mostly platinum (pink) and gold (light blue). Below the protection layer, the EDS maps of titania and oxygen (red and green) show the porous titania structure over the whole investigated area. For nickel (yellow) and, especially, sulfur (pink), the EDS map shows an increased signal close to the surface. This likely stems from an overlap of S K-lines with Au M-lines for S, and from an increased background signal, which is not fully removed, for Ni. However, the approximately constant signal for Ni and S

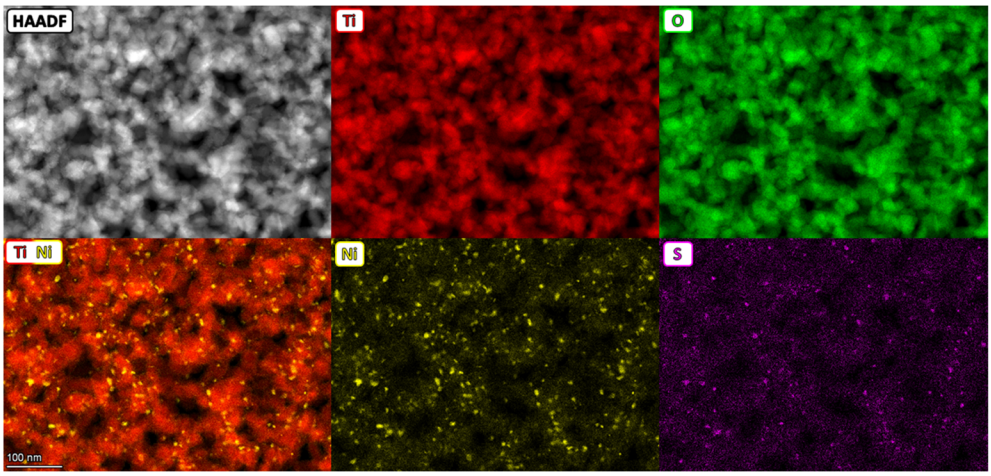

Fig. 3 HAADF-STEM images and EDS elemental maps of the sample cross section showing the homogeneously distributed nickel sulfide particles: titanum (red), oxygen (green), nickel (yellow), sulfur (pink).

throughout the bulk region of the sample indicates that the nickel xanthate precursor was able to infiltrate the whole titania layer during the deposition.

This is further confirmed in Fig. 4C, which shows a higher magnification image of the interface of the titania layer and the glass support (approximate area indicated by the rectangle C in Fig. 4B). The overlay of Ti/Ni/Si signals reveals small clusters of nickel sulfide distributed over the titania even near the interface to the glass substrate, with some visible Ni/S signal along the glass surface. This confirms that a successful deposition of NiS can be achieved *via* the xanthate route throughout at least 3 μm film thickness.

Film thickness and optical properties of NiS-modified titania

The TEM cross section analyses revealed a thickness of 3.2 μm for the specific investigated sample which is in good agreement with the thickness obtained by surface profilometry. This value is slightly higher than for the samples used later on in the photocatalytic experiments (2.7 μm). However, the film thickness, especially for the samples used for photocatalytic

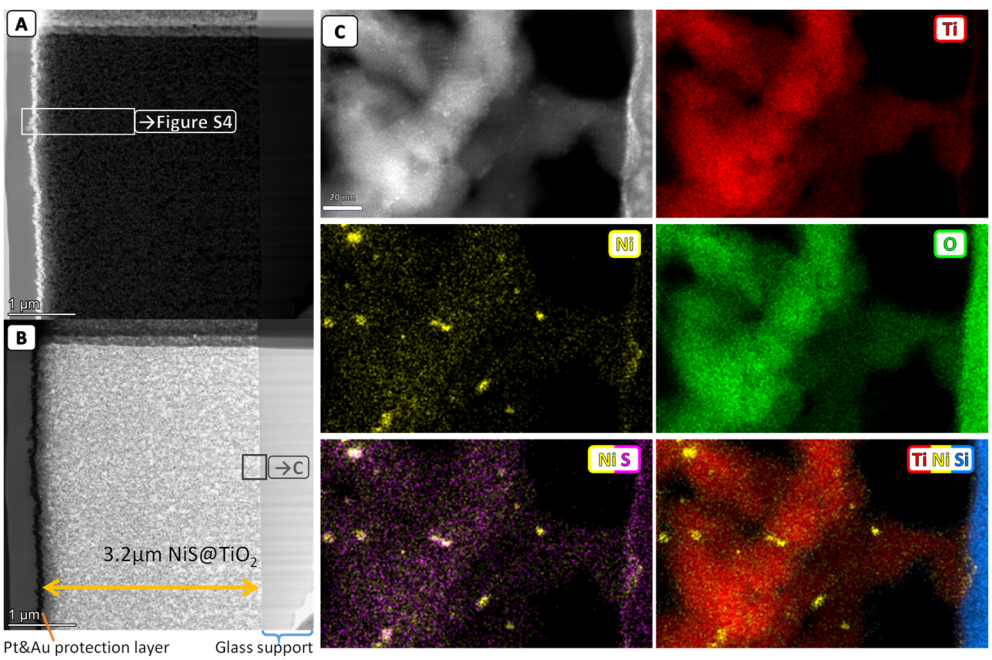

Fig. 4 STEM images of the sample cross section. (A) HAADF-image with the region for the elemental analysis (SI, Fig. S4) marked. (B) Bright field (BF) image of the same section. Different layers indicated: glass support, NiS@TiO_2, Pt & Au protection layer. (C) EDS elemental maps of the interface between titania and the glass support (region indicated in (B)). Top left to bottom right: HAADF-STEM, titanium (red), nickel (yellow), oxygen (green), overlay of nickel and sulfur (pink), overlay of titanium, nickel and silicon (blue).

experiments, can also be determined by a non-destructive measurement by UV-Vis spectroscopy. Constructive and destructive interferences of the reflectance contributions of both the glass support and the deposited titania thin film lead to a distinct interference pattern in the UV-Vis spectra (SI, Fig. S5A). Thus, the film thickness of a material with known refractive index can be calculated from the interference fringes, and *vice versa*.[38] However, the mesoporous nature of the titania film leads to a large deviation of the refractive index from compact titania.[39,40] Also, the refractive index of mesoporous titania itself can be tuned depending on the TiO_2 nanoparticle load in the organic template,[41] with reported values ranging from 1.6 (ref. 39) to 2.3.[40] Therefore, we correlated the film thickness measured by profilometry to the results obtained from the interference fringes to obtain the refractive index of our mesoporous titania layers. The obtained refractive index of 1.7 was then used to determine the film thicknesses of subsequent samples in a non-destructive fashion (SI, Fig. S5C and D). For the NiS@TiO_2 thin films used for the photocatalytic experiments, the thickness of the titania layer was determined to be 2.7 ± 0.1 μm (SI, Fig. S6D).

Furthermore, we recorded transmittance and diffuse reflectance spectra of titania thin films with different NiS loadings (SI, Fig. S6A and B). The absorption spectra, calculated from their corresponding transmittance and reflectance spectra, are shown in Fig. S6E. The optical band gap of the pristine titania thin film was obtained from a Tauc plot (SI, Fig. S6E inset) as the intersection of the *x*-axis and the extrapolation of the linear part. With 3.18 eV, the obtained optical band gap fits well to literature values for anatase. The thin films modified with NiS display a slight red shift of the absorption maximum and an increased light absorption into the visible spectral range up to approximately 600 nm. The NiS loadings were estimated using scanning electron microscopy – energy dispersive X-ray spectroscopy (SEM-EDS, SI, Fig. S7).

Hydrogen evolution reaction (HER)

Photocatalytic HER studies were conducted using temperature-controlled batch reactors directly on glass-supported NiS/TiO_2 films (details in Experimental). We chose the conditions for the HER experiments after considering preliminary tests (SI, Fig. S8) consisting of varying the excitation range (365 nm *vs.* 240–400 nm) and sacrificial electron donor (SED) (Na_2S/Na_2SO_3 *vs.* MeOH), and the illumination time (30 *vs.* 60 min). The light source was varied between a narrow-bandgap LED (centered at 365 ± 6 nm, power density of 238 mW cm^{-2}) and a broad-range Hg lamp (240–400 nm, 156 mW cm^{-2}), where the narrow-bandgap LED source proved to be more effective. Interestingly, while Na_2S/Na_2SO_3 SED is usually well suited to sulfide-based photocatalysts,[42] the use of aqueous MeOH solutions yielded higher H_2 production (SI, Fig. S8). We attribute this result to the fact that oxidation of the SED takes place on the TiO_2 surface, which is more suitable for MeOH adsorption. NiS takes the role of proton reduction sites, and therefore does not need to interact with the SED directly. We also note that in the first 30 minutes of the HER experiments, lower amounts of hydrogen were produced, while for the second 30 minutes of illumination a significant increase in H_2 values could be observed. This suggests that a dynamic catalyst activation process takes place in the beginning, possibly related to the reducing nature of Ni^{2+} species under photocatalytic conditions. A similar activation behavior of Ni@TiO_2 has been reported by Schubert *et al.*[43] Even though longer illumination times further increased the efficiency (as discussed later on), we chose 60 minutes as standard duration for the screening experiments to combine the increased efficiency with practical considerations of experimental time requirements.

Fig. 5A shows the photocatalytic H_2 evolution performance of different cocatalyst loadings prepared by varying the precursor concentration ranging from 20 to 340 μmol mL^{-1}. The pristine titania thin film showed almost no HER activity, which indicates that in the absence of a cocatalyst, there is rapid recombination of photogenerated charge carriers.[12] Also, the pristine NiS thin film showed no detectable HER activity (Fig. 5B), which highlights its limitations as stand-alone photocatalyst. In contrast to these results, the addition of the NiS cocatalyst to titania leads to a steep increase in HER activity, with approximately 100-fold higher HER rates achieved for the lowest NiS amount of about 0.6 w% (SI, Table S1). Upon further increase of the NiS amount, the HER activity increases, until a maximum efficiency is reached at 2.2 w% NiS (approximately 250-fold activity compared to pristine titania). Higher amounts of NiS than that lead to a decrease in the photocatalytic performance, likely resulting from a combination of factors: high amounts of NiS reduce the available oxidation sites on the TiO_2 surface, as well as having some shielding effect towards the light absorption of titania. Furthermore, aggregates of NiS can result in an increasing recombination of charge carriers within NiS.[12,44]

Benchmarking experiments (Fig. 5B) were carried out to compare the efficiency of our NiS@TiO_2 catalysts against platinum modified titania films. For this, pristine titania thin films were modified with two Pt loadings *via in situ* photo deposition (0.5 and 2.8%, w/w). Here, 0.5% represents the optimal loading for Pt/TiO_2 systems, while the 2.8% serves as a reference for the similarly loaded NiS/TiO_2 composite. The experiments with the cocatalyst amounts of 0.5 and 2.8% Pt yielded hydrogen generation rates of 4.6 and 6.1 mmol h^{-1} g^{-1}, respectively. This shows that the higher amount of 2.8% Pt (5.6-fold increase in Pt) is already in the region of cocatalyst overloading, as it yields only a 1.3-fold increase of the efficiency compared to the 0.5% platinum amount. Our best-performing NiS@TiO_2 with approximately 2.2% of NiS cocatalyst achieved a stunning 45% of the HER efficiency of the best-performing $Pt_{2.8\%}$@TiO_2 sample. Given the approximately 3000-fold difference in Pt price *vs.* Ni price (SI, Table S3, October 2025),[45,46] this result highlights the prospects of our xanthate-derived NiS cocatalysts for large-scale applications.

Finally, we evaluated the impact of the nickel xanthate precursor choice. Fig. 5C shows the average HER rate as a function of precursor type (using the same NiS loading) and highlights that tuning the chemistry of the Ni xanthate can lead to a variation – of approximately 30% – between the highest

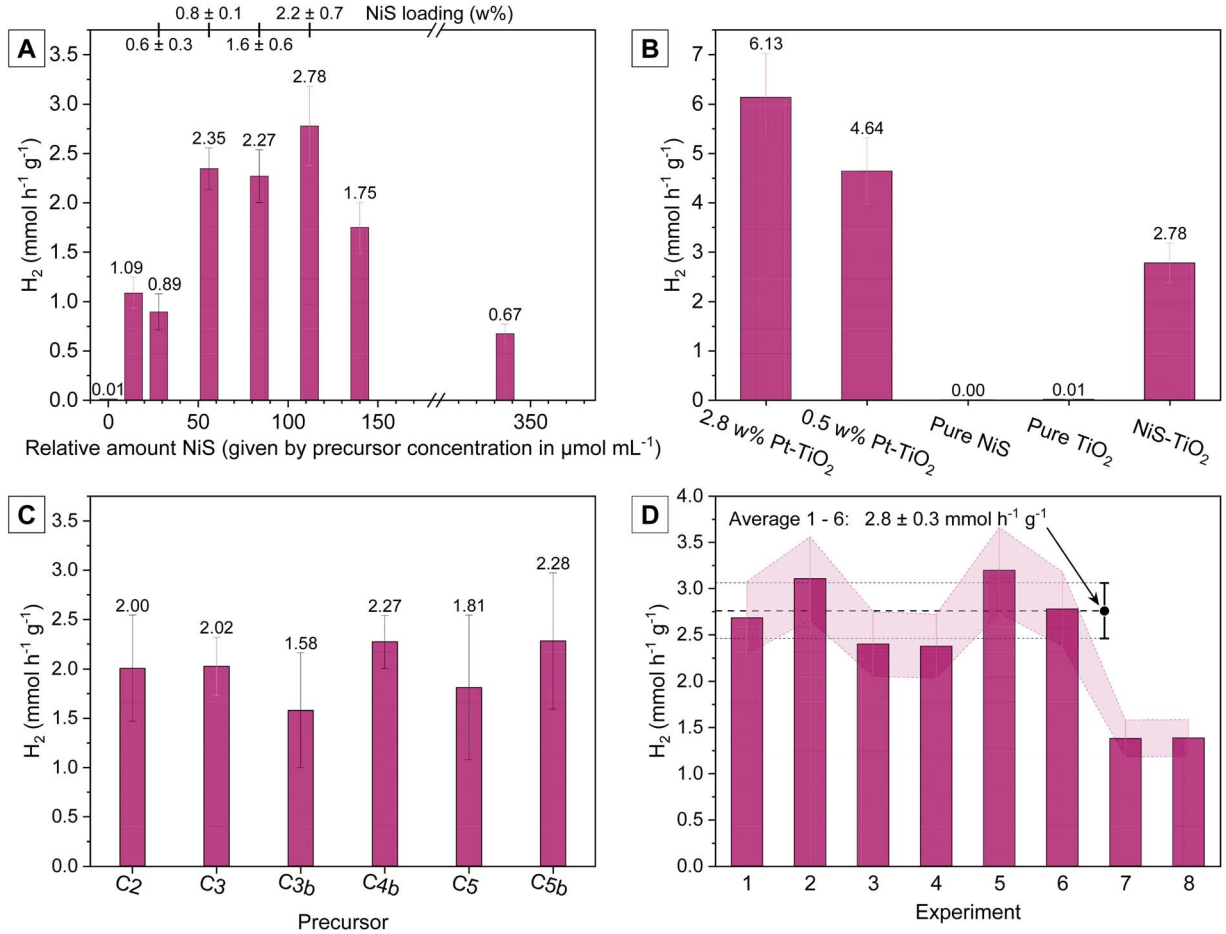

Fig. 5 (A) Evaluation of the influence of the NiS loading on mp-TiO_2 on the HER activity, NiXaC4b precursor was used for the preparation of the catalysts. For each loading, 3 measurements were conducted, but some measurements had to be excluded due to instrument issues. Error bars are given in black if 3 measurements for a specific sample were used for the calculation. Otherwise, pink error bars (using the overall experimental standard deviation of 14.5%) were added (SI, Fig. S9). (B) Reference HER experiments using mp-TiO_2 modified with two different loadings of Pt, pristine NiS, pristine mp-TiO_2, and NiS@TiO_2 with the best performing NiS loading (2.2 w%, precursor concentration: 110 µmol mL^{-1}). (C) Influence of the different nickel xanthate precursors on the HER activity using a precursor concentration of 84 µmol mL^{-1}. (D) Reusability of the catalysts evaluated by repeated one hour long HER runs (NiS loading: 110 µmol mL^{-1}) with overall experimental standard deviation included.

(prepared form NiXaC5b, but practically identical with NiXaC4b) and lowest (prepared from NiXaC3b) performing NiS/TiO_2 sample. Correlating these HER rates with the possible differences in NiS phase compositions (Fig. S2), it is possible to suggest that mixed NiS phases lead to higher-performing films: the NiS prepared from the precursors NiXaC3b and NiXaC5 yields phase-pure β-NiS, while all other precursors yield phase mixtures. This result is in good agreement with the findings of Shen *et al.*[16] who reported a higher hydrogen evolution rate when the photocatalyst $Cd_{0.5}Zn_{0.5}S$ was modified with mixed-phase α-NiS-β-NiS compared to pure β-NiS. More detailed evaluations of the influence of the alkyl groups on the xanthate's properties can be found in our previous work.[24]

HER stability experiments

The photocatalytic performance and stability of the NiS@TiO_2 catalysts was assessed in two ways: by repeated HER experiments using the same catalyst film (*i.e.* recyclability, Fig. 5D), and by conducting a long-time experiment with twenty hours continuous illumination (Fig. 6A). The recyclability experiment showed a good stability of the catalyst performance over multiple catalytic runs. For the first six experiments, an average efficiency of 2.8 ± 0.3 mmol h^{-1} g^{-1} was obtained, with some variability between measurements. The lower efficiency observed in the third/fourth runs compared to the second and fifth might be caused by hydrogen trapped as bubbles on the surface of the film, as the solution was not stirred during the experiment. After six experiments, the efficiency dropped to approximately half of the previous average. For the twenty hours experiment we could observe an average HER efficiency of 3.9 mmol h^{-1} g^{-1} for the best-performing timeframe (between three and sixteen hours), and an average evolution rate of 3.3 mmol h^{-1} g^{-1} over the whole experiment duration. This value is significantly higher than the result of the batch experiments, reaching 55% of the HER efficiency of the $Pt_{2.8\%}$@TiO_2 sample (or 330-fold activity compared to pristine titania). This might be explained by the continuous removal of the hydrogen

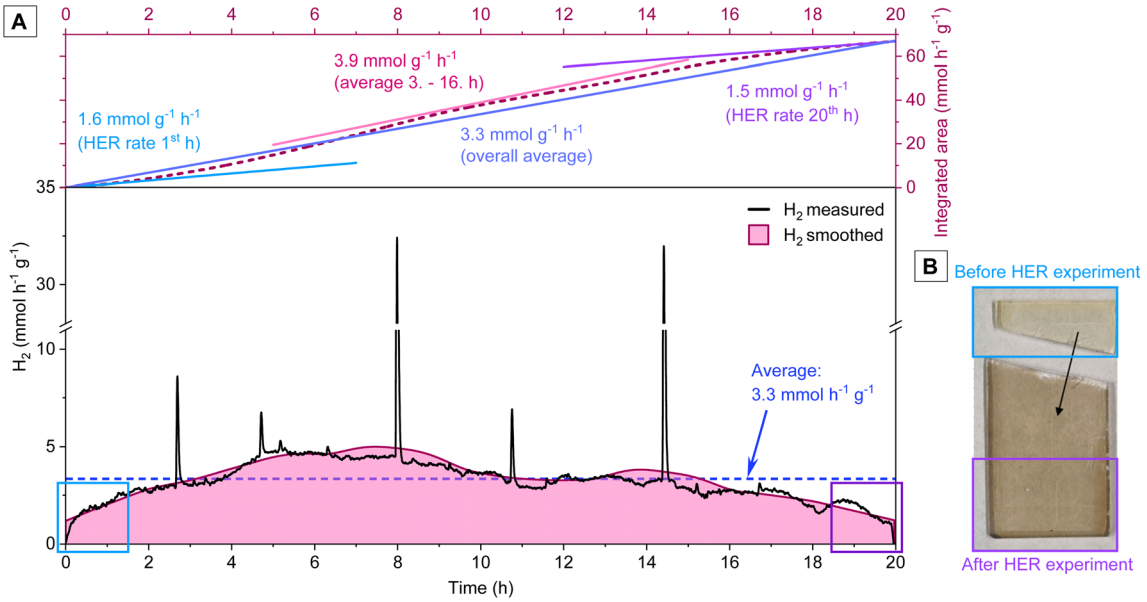

Fig. 6 (A) Stability of the catalysts evaluated by a long-time HER experiment over 20 hours, measurement is shown from the start of illumination. (B) Color change of the catalyst film during the HER experiment.

in the flow-setup. The removal of hydrogen from the gas phase provides a driving force for the dissolved hydrogen to enter the headspace, and, therefore, increases the observed efficiency.

In the beginning of the flow experiment, an increase of the efficiency can be observed, which can be attributed to the aforementioned catalyst activation,[43] with a peak performance attained after 6 hours of illumination. For the next approximately ten hours, the hydrogen evolution activity fluctuated slightly around the maximum with some activity spikes. These spikes can, again, be explained by the detachment of hydrogen bubbles from the surface of the titania film. In the last part of the experiment, a slow decrease of the activity was apparent as visualized by the diminished slope of the evolution rate shown on the top of Fig. 6A. While we note that our NiS/TiO_2 films keep being active even after 20 hours of illumination, this activation-deactivation behavior indicates a certain dynamics of this photocatalytic couple, which is also evident from the change of the film's color after the long-term experiment (Fig. 6B).

Investigation of the catalyst activation

The use of NiS@TiO_2 in thin film configuration allows us to study the reasons for the observed dynamics in photocatalytic activity in more detail. Fig. S10A (SI) shows UV-Vis spectra of the film before and after being exposed to UV light, revealing a strong rise in its absorbance over the entire UV-Vis range between 350 and 800 nm (SI, Fig. S10B). Interestingly, this color change is reversable. When the irradiated films are left in ambient air, the increased absorption reverts back to its original level within hours (SI, Fig. S10C). We suppose this reverse darkening-lightening of the film might be associated with the activation-deactivation behavior observed in the HER experiment. Given the experimental conditions, we suggest that the reversible darkening may originate from several processes: (i) a change in the titania component (*e.g.*, reduction of Ti^{4+} to Ti^{3+}), (ii) reduction of NiS and formation of NiS/Ni^0 during photocatalysis, or (iii) formation of $NiSO_4$ or NiO during photocatalysis, followed by hydroxide formation while in solution.

The formation of Ti^{3+} during photocatalysis could be excluded by cyclic voltammetry measurements (SI, Fig. S11–S13). During the CV measurements of a pure titania film, reversible Ti^{3+}-"self-doping" was observed, which has a characteristic bright blue color. In contrast, the same experiment using NiS-modified titania showed a slight brownish darkening of the film followed by gas evolution and a slightly higher current density. This discoloration was reversible also for the NiS-modified titania: in the reductive scan the film darkened, in the oxidative scan the color lightened up again (SI, Fig. S14). After the end of the cycling and drying of the film, the part of the film submerged in the electrolyte still had a slightly darker color than the not submerged part (SI, Fig. S13), which lightened after several tens of minutes in ambient conditions. Therefore, we suppose that the darkening of the film is more likely to stem from the nickel sulfide and not from the titania.

To test our second hypothesis, which involves the formation of metallic Ni, two samples were investigated using X-ray photoelectron spectroscopy (XPS). Fig. 7 shows the Ni 2p spectra for a pristine NiS@TiO_2 film (Fig. 7A), and a sample that had been illuminated in aqueous MeOH for 240 minutes (Fig. 7B). Additional XPS spectra (S 2p, Ti 2p, O 1s) are given in the SI (Fig. S16). However, we did not detect any signal from Ni^0, either before or after illumination. What we could observe from the XPS spectra were signals stemming from Ni–O or nickel oxysulfide. The Ni $2p_{1/2}$ and $2p_{3/2}$ signals are shifted to higher energies than expected for Ni–S, with only shoulders in the Ni $2p_{1/2}$ and Ni $2p_{3/2}$ signals indicating the presence of Ni–S. After argon sputtering to go deeper into the sample, the signals shift

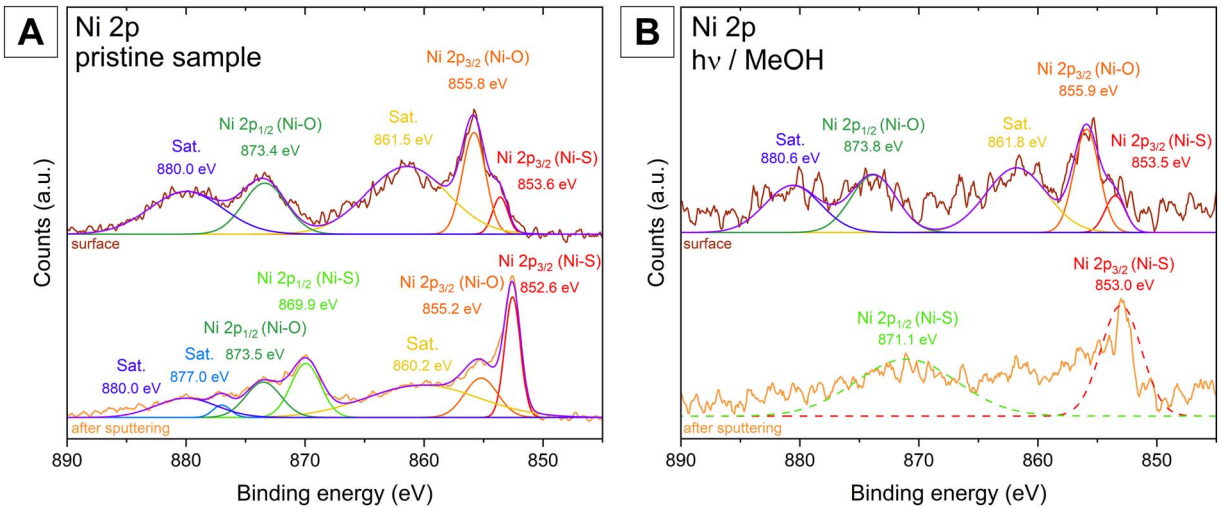

Fig. 7 High resolution XPS data of (A) an untreated NiS@TiO_2 film and (B) a NiS@TiO_2 film after UV illumination in water/MeOH solution, both films were prepared on a glass/FTO support. For both samples, spectra of the surface and spectra after removing the surface layer by argon sputtering are shown.

to a lower energy fitting to Ni–S. This indicates that the surface of the nickel sulfide nanoparticles is partially oxidized due to the contact with air.

Therefore, we tentatively suggest that the darkening might be correlated to the formation of $Ni(OH)_2$ at the surface of the sample, which is oxidized to NiOOH upon illumination in the aqueous MeOH solution. The film turning more transparent again some time after illumination might then be attributed to Ni^{3+} being reduced back to Ni^{2+}. Still, we cannot state that this is in direct correlation with the catalyst activation, but this is, in our opinion, the most likely reason for the observed reversable color change.

Conclusion

In this study, we prepared nickel sulfide modified mesoporous titania thin films using nickel xanthate single source precursors. By using these xanthate precursors in a simple solution processing method, we were able to easily prepare different loadings of NiS on titania for the modification of titania films. STEM and EDS maps of a sample cross section show homogeneously distributed NiS-nanoparticles throughout the whole thickness of the mesoporous film. UV-vis measurements showed an increased absorption in the visible range up to approximately 600 nm for the NiS-modified thin films compared to the pristine titania films.

We investigated the photocatalytic hydrogen evolution efficiency of NiS@TiO_2 thin films with different cocatalyst loadings using aqueous methanol as sacrificial electron donor. The NiS-modified photocatalyst showed a significantly enhanced photocatalytic activity compared to pure titania. We obtained the best results for a 2.2 w% loading of NiS, which showed a HER rate of 3.3 mmol h^{-1} g^{-1} averaged over a duration of 20 hours. This corresponds to a remarkable 55% of the HER efficiency of the best-performing $Pt_{2.8\%}$@TiO_2 sample. In addition, this HER rate is comparable to values reported for the NiS@TiO_2 system in suspension (SI, Table S2). A thin film photocatalyst, however, simplifies its use in continuous photocatalysis, as it removes the need for both stirring and separation present in a suspension system. While higher efficiency values for thin film photocatalysts have been published (SI, Table S2), our system presents a simpler fabrication compared to ternary systems. In addition, the use of a nickel sulfide cocatalyst makes our catalyst much cheaper than the highly efficient, but expensive noble metal based systems (SI, Table S3). These results suggest that our thin film catalysts could be used to assemble a low-cost and scalable photocatalytic continuous-flow set up to produce green hydrogen.

Ulrich Schubert tribute

This article is dedicated to Prof. Ulrich Schubert on the occasion of his 80th birthday, honoring his outstanding ability to inspire scientists in the field of materials chemistry through excellent research and teaching.

Experimental

All chemicals and solvents were purchased from commercial suppliers and used without any additional purification: 2-butanol (99%, VWR), carbon disulfide (≥99.9%, Sigma-Aldrich), chloroform (≥99.2%, VWR), diethyl ether (≥99.5%, Sigma-Aldrich), ethanol (99%, In-house), methanol (≥99.9%, VWR), neopentyl alcohol (99%, Thermo Scientific), nickel chloride hexahydrate (Sigma-Aldrich), 1-pentanol (≥99%, Sigma-Aldrich), 1-propanol (≥99%, VWR), 2-propanol (≥99.9%, Sigma-Aldrich), potassium hydroxide (≥85%, Roth), terpineol (mixture of isomers, 96%, Aldrich), 30 NR-D titania paste (Greatcell Solar Materials Pty Ltd).

Synthesis and thin film preparation

The xanthate precursors were synthesized according to previously published procedures.[37,47] In this work the precursors nickel(II) *O*-ethyl dithiocarbonate (NiXaC2), nickel(II) *O*-propyl dithiocarbonate (NiXaC3), nickel(II) *O*-isopropyl dithiocarbonate (NiXaC3b), nickel(II) *O*-isobutyl dithiocarbonate (NiXaC4b), nickel(II) *O*-pentyl dithiocarbonate (NiXaC5), and nickel(II) *O*-neopentyl dithiocarbonate (NiXaC5b) were used for the preparation of the cocatalyst.

The thin film photocatalysts were prepared on glass supports. Glass substrates were cut to the required size, cleaned by sonication in isopropanol for 30 minutes, followed by a treatment with oxygen plasma for 3 minutes (Femto low-pressure plasma system, Diener electronic). For the deposition of the mesoporous titania layer (mp-TiO_2), a commercial titania paste (Greatcell Solar Materials Pty Ltd, 30 NR-D) was diluted 1 : 1.5 w% with terpineol and stirred until a homogeneous mixture was obtained. The viscous paste was spread on the glass substrate with a spatula and spin coated at 3000 rpm, 1500 rpm/s for 45 seconds (WS-650MZ-23NPPB, Laurell Technologies), followed by pre-drying at 80 °C for 15 minutes and sintering at 500 °C for 15 minutes. A second layer was applied onto the first using the same procedure except for a longer annealing step of 60 minutes at 500 °C. The film thickness was determined using a profilometer and UV-Vis spectroscopy to be 2.7 μm (2.7 ± 0.1 μm). This preparation method proved to be highly reproducible regarding the film thickness. The titania films were modified with the nickel sulfide cocatalyst by spin coating a solution of nickel xanthate in chloroform (different concentrations and precursors). By default, the isobutyl derivative NiXa4b was used as precursor. 140 μL of the solution was applied and allowed to infiltrate the porous titania layer for 5 seconds. The surplus of solution was then removed by spin coating at 1800 rpm, 1500 s^{-2} for 45 s, followed by thermal conversion to nickel sulfide at 400 °C for 60 min under nitrogen atmosphere, yielding the final NiS@TiO_2 thin film catalyst.

Titania catalyst samples with different amounts of NiS were prepared by using different dilutions of the NiXaC4b precursor solution: 60 mg mL^{-1} (0.168 mmol mL^{-1}), 40 mg mL^{-1} (0.112 mmol mL^{-1}), 30 mg mL^{-1} (0.084 mmol mL^{-1}), 20 mg mL^{-1} (0.056 mmol mL^{-1}), 10 mg mL^{-1} (0.028 mmol mL^{-1}), 5 mg mL^{-1} (0.014 mmol mL^{-1}). For the evaluation of the effect of different precursors, the experiments for one concentration (0.084 mmol mL^{-1}) were also conducted with a range of precursors: NiXaC2 (25.3 mg mL^{-1}), NiXaC3 (27.6 mg mL^{-1}), NiXaC3b (27.6 mg mL^{-1}), NiXaC5 (32.3 mg mL^{-1}), NiXaC5b (32.3 mg mL^{-1}). The mass of the catalyst was determined by scraping off the titania layer and measuring on a microbalance to be 0.46 ± 0.05 mg cm^{-2} (1.51 ± 0.07 mg for the 15 × 25 mm^2 films, 3.11 ± 0.15 mg for the 25 × 25 mm films).

X-ray diffraction (XRD) measurements were taken on a RIGAKU MiniFlex 600 with D/Tex Ultra detector operated at 40 kV and 15 mA using CuK_α radiation ($\lambda = 1.5418$ Å).

Film thickness measurements were conducted on a DektakXT Profilometer from Bruker.

Optical characterization (UV-vis): absorption and reflectance spectra were recorded with a Shimadzu UV-2600i equipped with an ISR-2600Plus integrating sphere. Thin films for the optical characterization were prepared as described above: pristine titania films at different film thicknesses, NiS@TiO_2 thin films prepared from different concentrations of precursor solutions of the NiXaC4b precursor (0.112 mmol mL^{-1}, 0.056 mmol mL^{-1}, 0.028 mmol mL^{-1}, 0.014 mmol mL^{-1}).

Scanning transmission electron microscopy (STEM), energy dispersive X-ray spectroscopy (EDS) investigations were carried out on a probe corrected Titan³ G2 60-300 (FEI Company) operated at 300 kV with a field emission source (X-FEG) at a convergence angle of 19.6 mrad. A probe current of approximately 100 pA has been chosen. The microscope is equipped with a Super-X four-quadrant EDS detector. STEM images and EDS data was acquired and analyzed using the Velox software package (version 3.5). A cross section from the NiS@TiO_2 film on glass was prepared using focused ion beam. Prior to the preparation of the cross section a protection layer of gold and platinum was applied to the surface of the sample.

Particle size distribution of NiS particles was calculated based on Ni and S EDS elemental maps. Image segmentation was performed using the "pixel classification" workflow in the Ilastik software.[48] Further processing of the segmented images was done in ImageJ, where first touching particles were separated using the watershed algorithm before the area of all particles was calculated. This area is transformed into an equivalent diameter assuming circular particle shape.

The NiS loadings were estimated using scanning electron microscopy – energy dispersive X-ray spectroscopy (SEM-EDS). A Zeiss Sigma 300-VP SEM equipped with an Oxford $Xmax^N$ 80 EDS system was used, with the acceleration voltage set to 15 kV.

Hydrogen evolution reaction (HER): the thin film photocatalysts for the HER experiments were prepared on 1.5 × 2.5 cm glass supports as described above. The catalysts were submerged in an aqueous methanol solution (50% v/v MeOH) in a custom-built photoreactor (total volume of 32 mL) with inert atmosphere, water cooling for a constant temperature of 15 °C, and outside light exclusion. The reactor was purged with argon for 10 min at 10 mL min^{-1} and then irradiated with a monochromatic UV LED light source (centered at 365 ± 6 nm, power density of 238 mW cm^{-2}) or a broad-band emitting medium-pressure Hg lamp equipped with a cut off filter resulting in the photon range between 240 and 400 nm (power density of 156 mW cm^{-2}) for two to twenty-two hours without stirring. The H_2 evolution was monitored at different time intervals by sampling the headspace (300 μL) with a Shimadzu GC 2030 gas chromatography device equipped with a barrier ionization discharge detector and a Micropacked-ST column with He (6.0) as the carrier gas, calibrated using a 5-point calibration.

The samples were prepared and measured in triplicates, to obtain some statistical data. Some samples could not be measured due to errors during the experiment. No standard deviation is given for fewer than three measurements. The HER activity was normalized to mmol per h per gram of NiS@TiO_2 catalyst.

Cyclic voltammetry (CV) measurements were performed with a BioLogic SP-50 potentiostat/galvanostat and analyzed using ECLab software. A H-type photoelectrochemical cell (Ossila) was used with a three-electrode setup with a platinum wire counter electrode, an Ag/AgCl reference electrode (3M KCl) and a platinum plate electrode holder for the working electrode. The electrodes and the sample holder were purchased from Ossila. The films for CV measurements were prepared following the procedure described above on FTO conductive glass substrates.

The illumination for the photoelectrochemical investigation was performed with an OmniCure S200 UV curing system (Excelitas) with a high-power fiber light guide (lamp main spectral output: 350–450 nm, shutter activation latency: 50 ms).

X-ray photoelectron spectroscopy (XPS) characterizations were performed on a Nexsa G2 XPS system (Thermo Fisher Scientific Inc.) using a monochromatized Al Kα X-ray source. The analyzer was operated with a pass energy of 20 eV and a step size of 0.100 eV. The spectra were acquired without and with cleaning the sample surface by sputtering.

Author contributions

M. S. E.: conceptualization, data curation, formal analysis, synthesis and investigation, characterization methodology, project administration, visualization, writing – original draft, writing – review & editing. S. N. M.: conceptualization, data curation and investigation, writing – review & editing. M. S.: conceptualization, data curation, writing – review & editing. G. H.: data curation & investigation (transmission electron microscopy). M. N.: data curation & investigation (scanning electron microscopy). A. V.: data curation & investigation (X-ray photoelectron spectroscopy). T. G.: data curation & investigation (X-ray photoelectron spectroscopy). A. C. O.: investigation. A. C.: conceptualization, resources, writing – review & editing. D. E.: resources, writing – review & editing. T. R.: conceptualization, funding acquisition, supervision, writing – review & editing. G. T.: resources, conceptualization, funding acquisition, supervision, writing – review & editing.

Conflicts of interest

There are no conflicts to declare.

Data availability

All evaluated data is available in the manuscript. The data supporting this article (XRD, UV-Vis, TEM images, CV, XPS) is included as part of the supplementary information (SI). Additional information/data can be provided upon reasonable request. Supplementary information is available. See DOI: https://doi.org/10.1039/d5ta10299e.

Acknowledgements

The authors gratefully acknowledge the Graz University of Technology for financial support through the Lead Project *Porous Materials at Work for Sustainability* (LP-03).

References

1 IEA, *Global Hydrogen Review 2021*, Paris, 2021.
2 Y. Kim and H. Yang, *Energies*, 2025, **18**, 741.
3 M. Tao, J. A. Azzolini, E. B. Stechel, K. E. Ayers and T. I. Valdez, *J. Electrochem. Soc.*, 2022, **169**, 054503.
4 M. Nasser, T. F. Megahed, S. Ookawara and H. Hassan, *Environ. Sci. Pollut. Res.*, 2022, **29**, 86994–87018.
5 N. S. Lewis and D. G. Nocera, *Proc. Natl. Acad. Sci. U. S. A.*, 2006, **103**, 15729–15735.
6 H. Huang, B. Pradhan, J. Hofkens, M. B. J. Roeffaers and J. A. Steele, *ACS Energy Lett.*, 2020, **5**, 1107–1123.
7 Q. Wang and K. Domen, *Chem. Rev.*, 2020, **120**, 919–985.
8 S. Nishioka, F. E. Osterloh, X. Wang, T. E. Mallouk and K. Maeda, *Nat. Rev. Methods Primers*, 2023, **3**, 42.
9 M. Ni, M. K. H. Leung, D. Y. C. Leung and K. Sumathy, *Renew. Sustain. Energy Rev.*, 2007, **11**, 401–425.
10 I. Arora, H. Chawla, A. Chandra, S. Sagadevan and S. Garg, *Inorg. Chem. Commun.*, 2022, **143**, 109700.
11 Y. Ma, X. Wang, Y. Jia, X. Chen, H. Han and C. Li, *Chem. Rev.*, 2014, **114**, 9987–10043.
12 F. Xu, L. Zhang, B. Cheng and J. Yu, *ACS Sustain. Chem. Eng.*, 2018, **6**, 12291–12298.
13 S. Batool, S. P. Nandan, S. N. Myakala, A. Rajagopal, J. S. Schubert, P. Ayala, S. Naghdi, H. Saito, J. Bernardi, C. Streb, A. Cherevan and D. Eder, *ACS Catal.*, 2022, **12**, 6641–6650.
14 M. Hazra, M. Hofer, B. Fickl, A. Ertl, S. N. Myakala, D. Eder, S. Porcu, A. Cherevan, B. C. Bayer and P. C. Ricci, *Carbon*, 2025, **244**, 120678.
15 L. Wang and L. Zan, *J. Phys. Chem. Solids*, 2021, **150**, 109893.
16 L. Shen, S. Qi, Y. Jin, C. Li, J. Cheng, H. Wang, H. Ma and L. Li, *New J. Chem.*, 2022, **46**, 17469–17478.
17 D. Wu, F. Wang, Y. Tan and C. Li, *RSC Adv.*, 2016, **6**, 73522–73526.
18 C. Dong, Q. Chen, X. Deng, L. Jiang, H. Tan, Y. Zhou, J. Chen and R. Wang, *Inorg. Chem.*, 2024, **63**, 11125–11134.
19 Y.-N. Luo, Y. Li, L. Qian, X.-T. Wang, J. Wang and C.-W. Wang, *Mater. Res. Bull.*, 2020, **130**, 110945.
20 P. Mohammadyari and A. Nezamzadeh-Ejhieh, *RSC Adv.*, 2015, **5**, 75300–75310.
21 H. El-Hosainy, W. T. Alsaggaf, Z. I. Zaki and M. H. H. Mahmoud, *Opt. Mater.*, 2022, **133**, 113011.
22 Z. Meng, Y. Peng, W. Yu and Y. Qian, *Mater. Chem. Phys.*, 2002, **74**, 230–233.
23 A. Ghezelbash, M. B. Sigman and B. A. Korgel, *Nano Lett.*, 2004, **4**, 537–542.
24 M. S. Egger, M. Sigl, R. Saf, H. Amenitsch, A. Torvisco, T. Rath and G. Trimmel, *J. Mater. Chem. C*, 2025, **13**, 14301–14315.
25 C. Buchmaier, M. Glänzer, A. Torvisco, P. Poelt, K. Wewerka, B. Kunert, K. Gatterer, G. Trimmel and T. Rath, *J. Mater. Sci.*, 2017, **52**, 10898–10914.
26 P. D. McNaughter, J. Moore, S. G. Yeates and D. J. Lewis, *ACS Appl. Eng. Mater.*, 2024, **2**, 1225–1233.

27 H. C. Leventis, S. P. King, A. Sudlow, M. S. Hill, K. C. Molloy and S. A. Haque, *Nano Lett.*, 2010, **10**, 1253–1258.
28 T. Rath, M. Edler, W. Haas, A. Fischereder, S. Moscher, A. Schenk, R. Trattnig, M. Sezen, G. Mauthner, A. Pein, D. Meischler, K. Bartl, R. Saf, N. Bansal, S. A. Haque, F. Hofer, E. J. W. List and G. Trimmel, *Adv. Energy Mater.*, 2011, **1**, 1046–1050.
29 G. B. Shombe, M. D. Khan, C. Zequine, C. Zhao, R. K. Gupta and N. Revaprasadu, *Sci. Rep.*, 2020, **10**, 3260.
30 S. A. Alderhami, D. Collison, D. J. Lewis, P. D. McNaughter, P. O'Brien, B. F. Spencer, I. Vitorica-Yrezabal and G. Whitehead, *Dalton Trans.*, 2019, **48**, 15605–15612.
31 Y. T. Alharbi, F. Alam, A. Salhi, M. Missous and D. J. Lewis, *Sci. Rep.*, 2021, **11**, 3053.
32 M. Sigl, M. Egger, F. Warchomicka, D. Knez, M. Dienstleder, H. Amenitsch, G. Trimmel and T. Rath, *J. Mater. Chem. A*, 2024, **12**, 28965–28974.
33 J. Wang, J. Tian, P. Han, L. Song, W. Wang, K. Lin, D. Feng and B. Ma, *Langmuir*, 2024, **40**, 21161–21170.
34 M. Tasbihi, S. Kwon, B. Kim, D. Brüggemann, H. Hou, J. Lu, R. Amitrano, T. Grimm, J. García-Antón, P. Strasser, S. L. Riedel and M. Schwarze, *Langmuir*, 2024, **40**, 25800–25810.
35 N. Nalajala, K. K. Patra, P. A. Bharad and C. S. Gopinath, *RSC Adv.*, 2019, **9**, 6094–6100.
36 N. Banerjee, A. Roy and R. G. Nair, *Fuel*, 2026, **406**, 136920.
37 E. Vakalopoulou, C. Buchmaier, A. Pein, R. Saf, R. C. Fischer, A. Torvisco, F. Warchomicka, T. Rath and G. Trimmel, *Dalton Trans.*, 2020, **49**, 14564–14575.
38 A. R. Hind and L. Chomette, *The Determination of Thin Film Thickness Using Reflectance Spectroscopy (Publication Number SI-A-1205)*, Agilent Technologies Inc., 2011.
39 P. Karasiński, E. Gondek, S. Drewniak and I. V. Kityk, *J. Sol-Gel Sci. Technol.*, 2012, **61**, 355–361.
40 K. R. Phillips, T. Shirman, M. Aizenberg, G. T. England, N. Vogel and J. Aizenberg, *J. Mater. Chem. C*, 2020, **8**, 109–116.
41 C. Li, N. S. Colella and J. J. Watkins, *ACS Appl. Mater. Interfaces*, 2015, **7**, 13180–13188.
42 M. Wang, S. Shen, L. Li, Z. Tang and J. Yang, *J. Mater. Sci.*, 2017, **52**, 5155–5164.
43 J. S. Schubert, E. Doloszeski, P. Ayala, S. N. Myakala, J. Rath, B. Fickl, A. Giesriegl, D. H. Apaydin, B. C. Bayer, S. Kashiwaya, A. Cherevan and D. Eder, *Adv. Mater. Interfaces*, 2024, **11**, 2300695.
44 H. Gu, Z. Lin, Y. Li, D. Wang and H. Feng, *Phys. Status Solidi A*, 2024, 2400187.
45 Trading Economics, Nickel, https://tradingeconomics.com/commodity/nickel, accessed October 24, 2025.
46 Trading Economics, Platinum, https://tradingeconomics.com/commodity/platinum, accessed October 24, 2025.
47 E. Vakalopoulou, T. Rath, M. Kräuter, A. Torvisco, R. C. Fischer, B. Kunert, R. Resel, H. Schröttner, A. M. Coclite, H. Amenitsch and G. Trimmel, *ACS Appl. Nano Mater.*, 2022, **5**, 1508–1520.
48 S. Berg, D. Kutra, T. Kroeger, C. N. Straehle, B. X. Kausler, C. Haubold, M. Schiegg, J. Ales, T. Beier, M. Rudy, K. Eren, J. I. Cervantes, B. Xu, F. Beuttenmueller, A. Wolny, C. Zhang, U. Koethe, F. A. Hamprecht and A. Kreshuk, *Nat. Methods*, 2019, **16**, 1226–1232.